Hindawi
Mathematical Problems in Engineering
Volume 2021, Article ID 6668942, 10 pages
https://doi.org/10.1155/2021/6668942

Research Article

Computational Fluid Dynamics Analysis of Impingement Heat Transfer in an Inline Array of Multiple Jets

Parampreet Singh,[1] Neel Kanth Grover,[2] Vivek Agarwal,[2] Shubham Sharma,[2] Jujhar Singh,[2] Milad Sadeghzadeh,[3] and Alibek Issakhov[4]

[1]*Department of Mechanical Engineering, Dr. BR Ambedkar National Institute of Technology, Jalandhar, India*
[2]*Department of Mechanical Engineering, IK Gujral Punjab Technical University, Main Campus-Kapurthala, Kapurthala, India*
[3]*Department of Renewable Energy and Environmental Engineering, University of Tehran, Tehran, Iran*
[4]*Faculty of Mechanics and Mathematics, Department of Mathematical and Computer Modelling, Al-Farabi Kazakh National University, Almaty, Kazakhstan*

Correspondence should be addressed to Milad Sadeghzadeh; milad.sadeghzadeh@gmail.com

Received 19 November 2020; Revised 21 December 2020; Accepted 30 March 2021; Published 13 April 2021

Academic Editor: Alessandro Mauro

Amid all convective heat transfer augmentation methods employing single phase, jet impingement heat transfer delivers significantly higher coefficient of local heat transfer. The arrangement leading to nine jets in square array has been used to cool a plate maintained at constant heat flux. Numerical study has been carried out using RANS-based turbulence modeling in commercial CFD Fluent software. The turbulent models used for the study are three different "*k*-*ε*" models (STD, RNG, and realizable) and SST "*k*-*ω*" model. The numerical simulation output is equated with the experimental results to find out the most accurate turbulence model. The impact of variation of Reynolds number, inter-jet spacing, and separation distance has been considered for the geometry considered. These parameters affect the coefficient of heat transfer, temperature, and turbulent kinetic energy related to flow. The local "h" values have been noticed to decline with the rise in separation distance "H/*D*." The SST "*k*-*ω*" model has been noticed to be in maximum agreement with the experimental results. The average value of heat transfer coefficient "h" reduces from 210 to 193 W/m^{2}K with increase in "H/*D*" from 6 to 10 at "Re" = 9000 and S/*D* of 3. As per numerical results, inter-jet spacing "S/*D*" of 3 has been determined to be the most optimum value.

1. Introduction

The application of jet impingement because of its higher convection heat transfer rates in processes, namely, mechanical as well as chemical, has steered numerous industry applications, for instance, metal plates cooling/heating, cooling of turbine blades, industrial equipment cleaning, and cooling of Micro Electro Mechanical Systems (MEMS). Jet impingement is normally utilized in numerous industrial applications which include automobile windshield de-icing, electronic component cooling, and glassware. High convective transfer rates associated with the jet impingement has ensured the use of this technology in the fields where the heat fluxes associated are very high and the space is restricted. Heat, Ventilation, and Air-Conditioning (HVAC) is significant for building indoors, not only for adequate comfort levels and quality of air for occupants, but also in terms of the energy consumption [1–3]. Impinging Jet Ventilation (IJV) is the new technique emerging in this field which uses the idea of an impinging jet employed for cooling a heated target surface. Good number of experimental, numerical, and analytical studies have been performed. Outstanding review papers (Viskanta [4] and Zuckerman and Lior [5]) have been published with an emphasis on different issues. The transfer of heat from a single striking jet is bell shaped Gaussian distribution and thus can lead to the formation of hot spots on target surface [4, 5]. Thus, it has been established that multiple impinging jets can give rise to

better heat transfer consistency at the impingement surface. Interactions and thermal characteristics developed in multiple conventional striking jets (MCIJs) have been extensively explored. In multiple jet impingement, each impinging jet may be influenced essentially by two different kinds of interactions. First are inter-jet interactions preceding their impingement on the surface. This type of interaction is important in geometries having small inter-jet spacing and large separation distances. Second type is interaction among the wall jets of impinging jets after their impingement on surface. These primarily occur for array configurations with smaller inter-jet spacing with high velocities.

Metzger and Korstad [6] experimentally determined the effect of cross flow in multiple impinging jets on a horizontal plate. Inline circular jets with varying inter-nozzle distance and separation distance among jets and impingement plate were studied. Heat transfer coefficient is controlled with jet-diameter Reynolds number and inter-jet spacing. Li et al. [7] explored heat transfer from triangular array of jets with varying diameters on a roughened target surface. Goldstein and Timmers [8] studied a geometry of single jet bounded by a hexagonal array of six circular jets with radius of 5 mm. Behbahani and Goldstein [9] stated that at a fixed mass flow rate per jet, decreasing inter-jet spacing resulted in increased area averaged Nusselt number. Experiments carried out by Florschuetz et al. [10] indicated the direct advantages of reducing jet diameter as well as letting free space among jets for directing the spent gas flow. Obot and Trabold [11] examined effects of cross flow employing geometries with minimum, intermediate, and maximum crossflow. Goldstein and Seol [12] stated that local Nusselt number should be higher at smaller separation distance ($H/D = 2$) than at larger distance of $H/D = 6$. Slayzak et al. [13] investigated the interactions between adjacent jets using a twin jet impingement system. By varying the momentum of twin jets, oscillations were observed in the interaction zone. For a round jet at "H/D" = 2, Huber and Viskanta [14] noticed a peak in local "Nu" for a ring formed region around "r/D" = 0.5 and a second smaller peak at "r/D" = 1.6. San and Lai [15] showed that interaction between the jets produced smaller peaks in heat transfer distribution among the stagnation regions because of interactions among neighbouring jets. Geers et al. [16, 17] studied velocity flow field for the multiple array of circular jets striking on a flat horizontal plate. Results revealed interactions taking place among cross flow as well as the wall jets that led to the development of horseshoe vortices. Spring et al. [18] stated that inline arrangement is superior to staggered arrangement of jets mainly attributed to the nature of crossflow existing in the array. San and Chen [19] reported that for the rise of separation distance from 0.5 to 2, the Nusselt number maxima between central and neighbouring jets disappeared attributed mainly to the decreased interactions between adjacent jets. Florschuetz et al. [20] studied the crossflow effects with temperature difference between crossflow and impinging jets. Gardon and Akfirat [21] conducted experiments on slot jet array and presented that the definition of each jet is maintained and the peak values in heat transfer distribution differed slightly from those pertaining to single impinging jets. Lee and Lee [22] established that orifice nozzles lead to high rates of heat transfer rates in comparison to fully developed pipe flow. Weigand et al. [23] conducted experiments on multiple jet impingement instead of a single jet and determined the presence of secondary stagnation zones and vortices that result in the reduction of heat transfer rates. This flow of gas is called spent gas and these wall jets are predominant in the geometries where the small inter-jet spacing, small gap distances among nozzle plate and target plate, and large velocities are used. Chougule et al. [24] determined experimentally that the rise in "H/D" resulted in decreased heat transfer rates. Higher heat transfer rates are visible in lower "H/D" ratios because of the decrease in the impact area as the jet does not mix well with the ambient fluid. Yong et al. [25] experimentally studied the crossflow effects of spent gases in staggered and inline array schemes and demonstrated that the effects of crossflow from upstream rows of jets to downstream rows are more pronounced for a staggered array in contrast to an inline array. Computational fluid dynamics has now emerged as a powerful tool for predicting the flow situations and heat transfer characteristics. Likewise, heat transfer enhancement is also gaining popularity so as to increase the thermal performance of the systems. There are many studies conducted where heat transfer enhancement has been studied by utilizing nano-sized particles and V-ribs for solar panels [26–33]. Jet impingement also focusses on the enhancement of heat transfer using turbulence induced mixing as a means for increased heat transfer coefficient.

The literature review suggests that there are few studies available in which the effects of interactions in larger arrays of impinging jets have been investigated numerically for heat transfer characteristics. Based on this finding, the present work has been performed where an inline array of nine impinging jets has been investigated for studying the impact of interactions upon heat transfer characteristics at different inter-jet spacings ("S/D" = 2, 3, 5, and 7), separation distances ("H/D" = 6, 8, and 10), and Reynolds numbers ("Re" = 7000, 9000, and 11000).

2. Numerical Modeling

The three-dimensional flow situation has been solved using the Navier–Stokes and energy equations along with turbulence models by means of CFD software (FLUENT 6.3.26) to predict the thermal and turbulent flow fields for the flow physics. Equations (1)–(5) have been solved in the commercial Fluent CFD code [34]. The "k-ω" turbulence model has been used with shear stress transport (SST) option, and it has been found to work best for wall bounded flows than other turbulence models available. The "k-ω" turbulence model is selected because of its lesser computation requirements, simplicity, and worldwide acceptability. The flow has been considered as incompressible for the sake of simplicity, and steady-state conditions have been assumed. The gravity and radiation heating are neglected, and temperature dependence for standard thermophysical properties such as specific heat, density, and heat conductivity has

also not been considered. Figure 1(a) illustrates the detail description of the problem with the application of boundary conditions. The bottom wall of computational domain has been given a constant heat flux condition. Nine nozzles, having diameter "D" = 5 mm and length "L" = 25 mm, have been used to supply air in the form of round air jets. The velocity of the air jets has been varied with the use of different Reynolds number. These air jets exit the domain after impingement from the pressure outlets given at the sides of the domain. Likewise, the nozzle plate at the top has been assigned the constant temperature boundary condition. This plate also acts as a semiconfinement for the impinging jets. The schematic details of nozzle plate are given in Figure 1(b) for jet spacing of 15 mm corresponding to nondimensional distance of S/D = 3. The target plate has been maintained at a static heat input rate of 30 W, and all other surfaces except for the top surface are considered to be adiabatic. The governing equations for momentum, pressure, turbulent kinetic energy, specific rate of dissipation, and energy have been discretized using second-order techniques. A tetrahedral meshing scheme having y^+ values less than five and adequate near wall treatment has been employed around wall region so as to precisely resolve viscous sublayer region.

The velocity inlet boundary condition has been specified with the value of measured velocity from the Reynolds number, and static temperature of 300 K has also been assigned at the velocity inlet. No-slip criteria have been implemented at the wall surface for viscous effects. The pressure outlet boundary condition signifies the outflow of the spent flow, and it corresponds to the far field flow conditions with temperature (300 K), gauge pressure of "0" Pa relating to atmospheric conditions, and turbulence intensity of 5%. For the impingement wall, a uniform heat flux of 8333 W/m^2 (30 W for 60 × 60 mm plate) has been specified along with temperature value of 40°C at bottom surface of heat sink. The other heat sink sides are taken to be adiabatic. The temperature values thus obtained at the top surface of base plate have been appended to the computational flow domain, and simulations have been carried out with different conditions of varying inter-jet spacings, H/D, and Reynolds number.

To minimize the computational time and efforts, only quarter of the complete domain is modeled, and by using symmetry boundary conditions, the heat transfer and fluid flow characteristics can be accurately predicted. Figure 2 portrays the computational grid generated for numerical study, and Table 1 highlights different boundary conditions given at various sides of the flow domain. Numbers of cells used for the quarter domain are around 4,34,000, thus resulting in 1.7 million cells for the complete domain which are adequate to model the fluid flow. To minimize the computational efforts, thermophysical properties for air have been approximated to be constant. The SIMPLE algorithm aimed at pressure velocity coupling has been taken for solving the pressure field [34]. The convergence criterion used for residuals in momentum, energy, and turbulence parameters has been specified as 10^{-6}. The numerical calculations have been performed on a computer system having the following configuration: Intel i3 (4 core) processor, 4 GB RAM, 512 GB HDD, and 2 GB graphics. The computation time that has been taken by the computer in solving different mesh sizes is given in Table 2.

2.1. Numerical Procedure. CFD study of the multi nozzle impingement has been conducted by solving the discretized equations of mass, momentum, and energy conservation (equations (1)–(3)). RANS-based momentum equations have been solved for obtaining the flow velocities under steady-state conditions.

2.1.1. Continuity Equation.

$$\nabla.(\rho\vec{V}) = 0. \tag{1}$$

2.1.2. Momentum Equation.

$$\nabla.(\rho\vec{V}\vec{V}) = -\nabla p + \nabla.\left(\mu_{\text{eff}}\nabla\vec{V}\right). \tag{2}$$

2.1.3. Energy Equation. The energy equation is solved to obtain the temperature data in the flow field.

$$\nabla.(\vec{V}(\rho E + p)) = \nabla.\left(k_{\text{eff}}\nabla T - \sum_{j=1}^{N} h_j \vec{J}_j\right). \tag{3}$$

2.1.4. Turbulence Parameters. The turbulence in the flow has been numerically solved using two turbulence models, and the equations used for solving the turbulence parameters are given in equations (4)–(7). The turbulence parameters are calculated or predicted as per the model being used so as to calculate the value of turbulent viscosity which is then used to estimate the value of effective viscosity in equation (2). With the inclusion of this term, the velocity field can be calculated numerically as the equations are now mathematically closed. Equations (4) and (5) represent the transport equations for turbulent kinetic energy (k) and dissipation rate (ε) as used in k-ε models. Likewise, the turbulent parameters (k) and specific dissipation rate (ω) have been estimated for k-ω model as per equations (6) and (7).

$$\nabla(\rho k\vec{V}) = \nabla\left[\alpha_k\mu_{\text{eff}}\nabla k\right] + G_k - \rho\varepsilon, \tag{4}$$

$$\nabla(\rho\varepsilon\vec{V}) = \nabla\left[\alpha_\varepsilon\mu_{\text{eff}}\nabla\varepsilon\right] + C_{1\varepsilon}\frac{\varepsilon}{k}G_k - C_{2\varepsilon}\rho\frac{\varepsilon^2}{k} - R_\varepsilon, \tag{5}$$

$$\nabla(\rho k\vec{V}) = \nabla\left[\alpha_\varepsilon\mu_{\text{eff}}\nabla k\right] + G_k - Y_k + S_k, \tag{6}$$

$$\nabla(\rho\omega\vec{V}) = \nabla\left[\alpha_\varepsilon\mu_{\text{eff}}\nabla\omega\right] + G_\omega - Y_\omega + S_\omega. \tag{7}$$

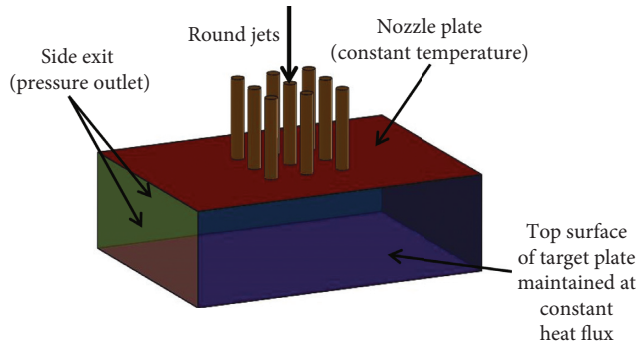

Figure 1: Physical description and boundary conditions at various surfaces.

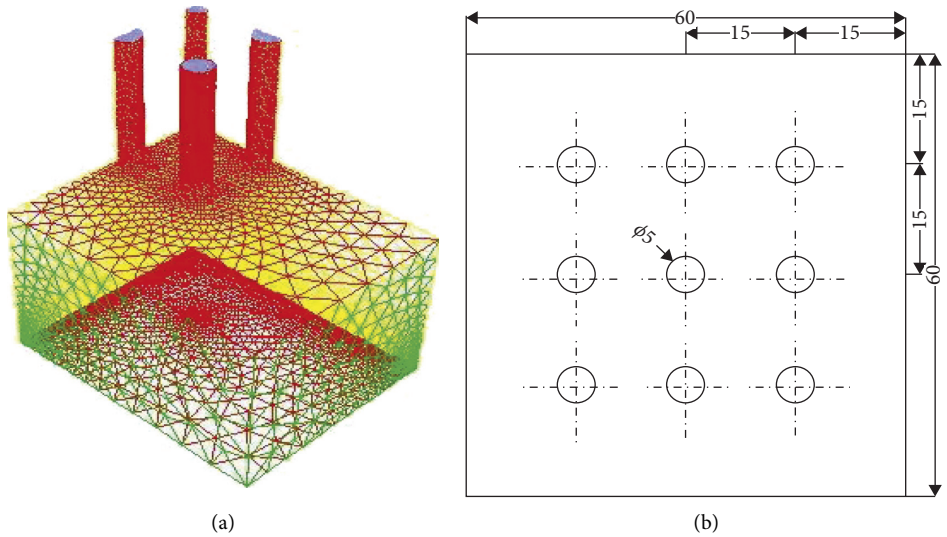

Figure 2: (a) Computational mesh generated for the numerical computation and (b) schematic view of nozzle plate being used.

3. Numerical Results

Numerical study has been executed to explore the impact of variation in "S/*D*," "H/*D*," and "Re" upon heat transfer characteristics. For the validation of numerical results, Table 3 highlights the average heat transfer coefficient values compared to the experimental output of Chougule et al. [24] along with the errors at fixed conditions corresponding to "H/*D*" of 8, S/*D* of 3, and Re of 9000. On the basis of these results, *k*-*ω* "SST" model has been implemented for numerical simulations. Likewise, local coefficient of heat transfer has also been plotted against nondimensional distance along *x*-axis (Figure 3) for "H/*D*" = 6 and Re = 9000.

3.1. Impact of Separation Distance (H/D). The impact of separation distance (H/*D*) among the nozzle and the target plate has been explored by varying "H/*D*" at the same "S/*D*" and Reynolds number. The rise in separation distance resulted in decreased rate of heat transfer as the increase in the separation improves the interaction among the jets and the surroundings, and thus velocity of the jet decreases owing to increased momentum exchange. The values of coefficient of heat transfer as well as Nusselt number should thus decline at stagnation regions. Figure 4 shows the distribution of heat transfer coefficient and turbulent kinetic energy (TKE) at Reynolds number "Re" = 7000 for numerous values of separation distances ("H/*D*" = 6, 8, and 10) for "*D*" = 5 mm.

The values of local "h" decrease with increasing "H/*D*" at the stagnation region pertaining to the jet at "X/*D*" = 0. The variation shows value of "h" to decrease from 390 W/m^2-K to 270 W/m^2-K as "H/*D*" is increased from 6 to 10.

The value of peak in "TKE" distribution reduces from 15 m^2/s^2 to 2 m^2/s^2 for the separation distance "H/*D*" changing from 6 to 10. Likewise, Figures 5 and 6 portray local "h" and "TKE" distribution intended for different "H/*D*" at fixed "S/*D*" of 3 and Re of 9000 and 11000.

The values of local heat transfer coefficient and turbulent kinetic energy can be seen to be increasing with increasing Reynolds number since the increase in flow velocities tends to increase the turbulent interactions with the atmosphere. The increase in axial flow velocities also results in lesser jet spread and thus lesser thermal dilution leading to higher heat transfer. At the interaction region formed in-between adjacent jets (i.e., "X/*D*" ~ 1.5), the higher flow velocities of wall

Table 1: Boundary conditions used for computation.

Physical location/identity	Boundary type	Mathematical representation
Top plate/nozzle plate	Wall	$u = v = w = 0$; $T_s = 300$ K
Bottom surface/impingement plate	Wall	$u = v = w = 0$; $q'' = 8333$ W/m^2
Side/opening/outlet	Pressure outlet	$P = P_{atm}$
Rear/side surface	Symmetry	$\partial(.)/\partial x_j = 0$
Inlet/velocity inlet	Velocity inlet	As per value of Re at the nozzle
Nozzle walls	Wall	$u = v = w = 0$; $T = 300$ K

Table 2: Computational grids and time taken for convergence.

S. No.	Mesh density/size	Computational time
1	301,720 cells	6 hours (approx.)
2	4,34,000 cells	9 hours (approx.)
3	6,55,600 cells	11 hours 30 minutes (approx.)

Table 3: Comparison of different turbulence models.

Sr. No.	Turbulence models	Average heat transfer coefficient (h)	Error (% age)
1	Experimental value	210 W/m^2-K	—
2	k-ε STD	181 W/m^2-K	13.8
3	k-ε RNG	192 W/m^2-K	8.57
4	k-ε realizable	191 W/m^2-K	9.04
5	k-ω SST	204 W/m^2-K	2.85

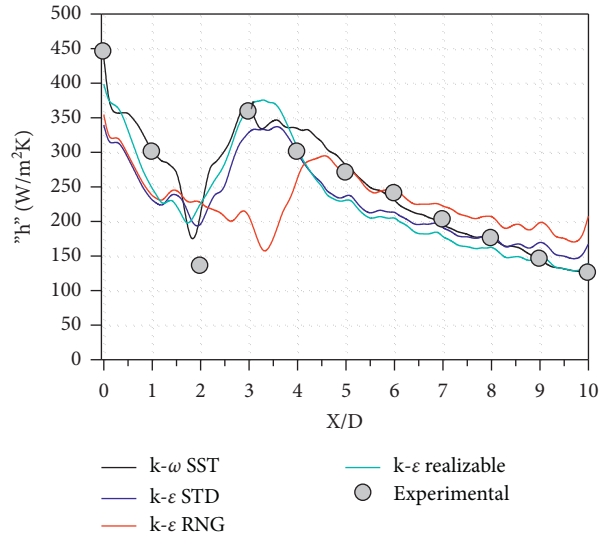

Figure 3: Local heat transfer coefficient (W/m^2-K) distribution with respect to "X/D" for various turbulence models.

jets result in flow separation in form of fountain upwash flow. Due to this flow separation, the value of "h" at this region is very less. One more observation can be made for "H/D" = 10 case that the stagnation region formed here ("X/D" = 0) shows a plateau of high local "h" values instead of depicting a sharp peak as seen for "H/D" = 6 and 8. This happens due to increased jet spread taking place due to the increased space available between nozzle exit and impingement plate for higher separations.

3.2. Impact of Inter-Jet Spacing (S/D). The values of "S/D" considered for the present analysis are "S/D" = 2, 3, 5, and 7. These "S/D" values are sufficient to analyze how the jets will behave for very close, medium, and far inter-jet spacings. The increase in "S/D" will result in decreased interactions among the jets, and therefore the total heat transfer will decrease and the decrease in "S/D" will lead to increased interaction and thus increase in heat transfer. The too small value of "S/D" resulted in array of jets to behave like a large single jet, and thus the heat transfer coefficient value is also high, but study of interaction effects cannot be made properly. The impact of variation in inter-jet spacing is depicted graphically in Figure 7. The graphs show the variation in heat transfer coefficient and temperature at central horizontal axis of the target plate for the nine jets at "S/D" = 2, 3, 5, and 7 for fixed value of Reynolds number, "Re" = 9000, "H/D" = 8, and "D" = 5 mm.

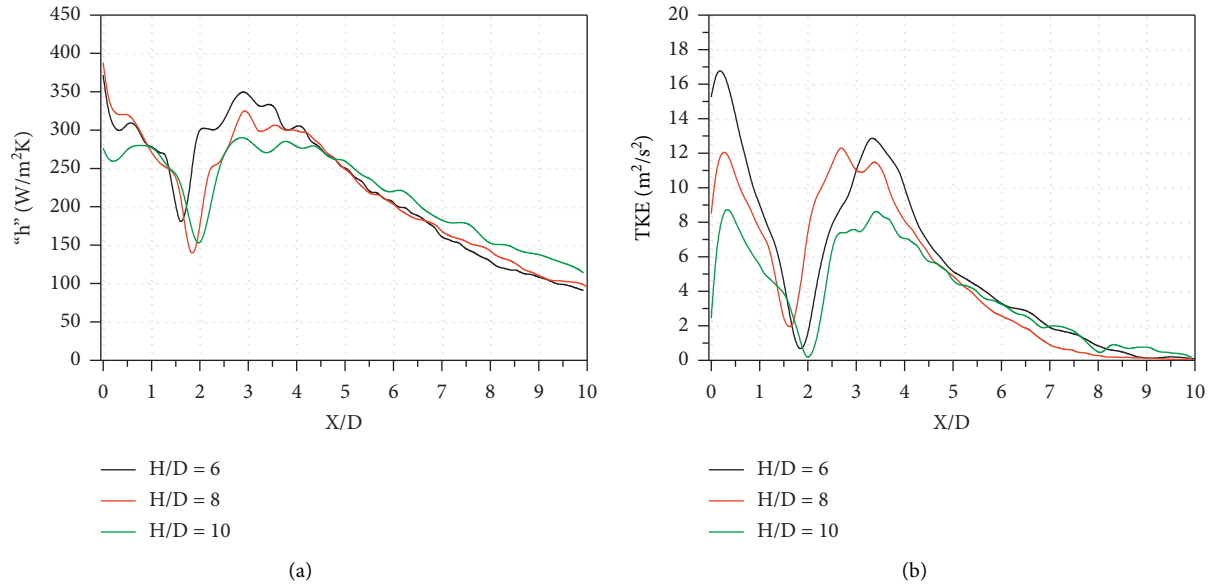

Figure 4: (a) Local heat transfer coefficient (W/m^2-K) and (b) turbulent kinetic energy (m^2/s^2) distribution at fixed "S/*D*" of 3 and "Re" of 7000 for varying separation distances, "H/*D*" of 6, 8, and 10.

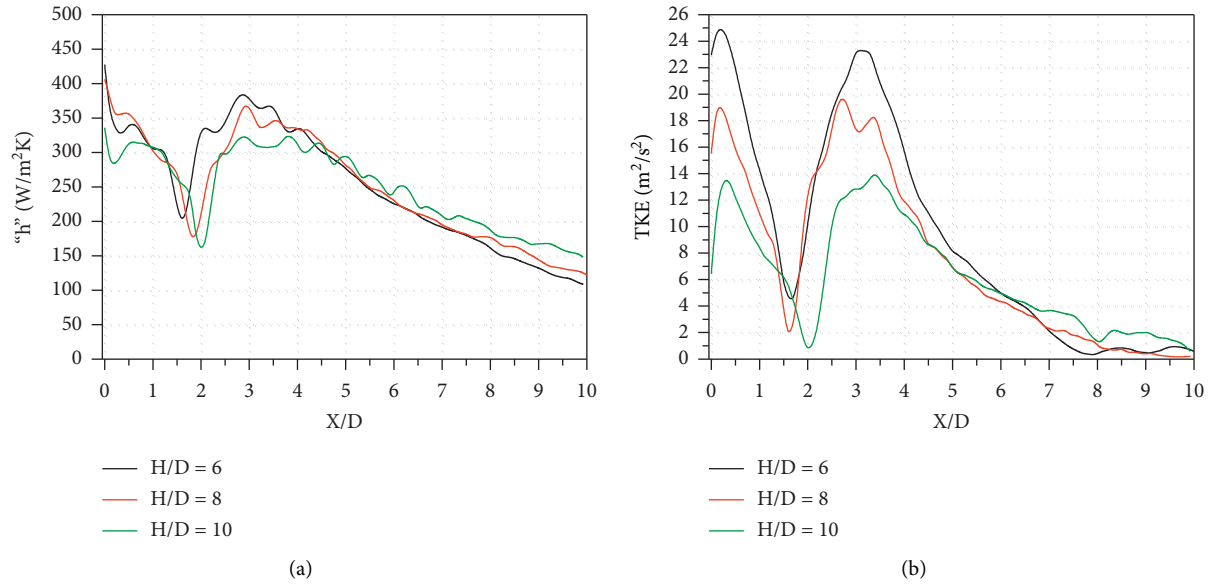

Figure 5: (a) Local heat transfer coefficient (W/m^2-K) and (b) turbulent kinetic energy (m^2/s^2) distribution at fixed "S/*D*" of 3 and "Re" of 9000 for varying separation distances, "H/*D*" of 6, 8, and 10.

Figure 7 shows declining tendencies for the change in heat transfer coefficient by increasing "S/*D*." This reduction in the values of heat transfer coefficient "h" can be anticipated due to decrease in the interaction among the neighbouring jets. At lower values of "S/*D*," the interaction between the jets and lesser spacing results in turbulence and thus increase in heat transfer rates. As the value of "S/*D*" increases, the distance among the jets increases, and thus the rate of heat transfer per unit area decreases. Figure 7 also shows the variation in temperature with respect to "X/*D*." The values of temperature are found to rise with the rise in "S/*D*" at "X/*D*" = 0. Also, the local maxima developed at the interaction region in-between adjacent jets can be seen to show an increase in temperature values with the rise in the value of inter-jet spacing "S/*D*." This is due to the decreased interactions and lesser heat transfer taking place in the interaction region for different "S/*D*" cases here. The decrease in heat transfer leads the surface plate temperature to rise, and thus the cooling of plate is not effective at these interaction regions.

3.3. Impact of Reynolds Number (Re). Impact of Reynolds number on the heat transfer rate has been studied at fixed "H/*D*" of 6 and "S/*D*" of 3, and Reynolds number has been

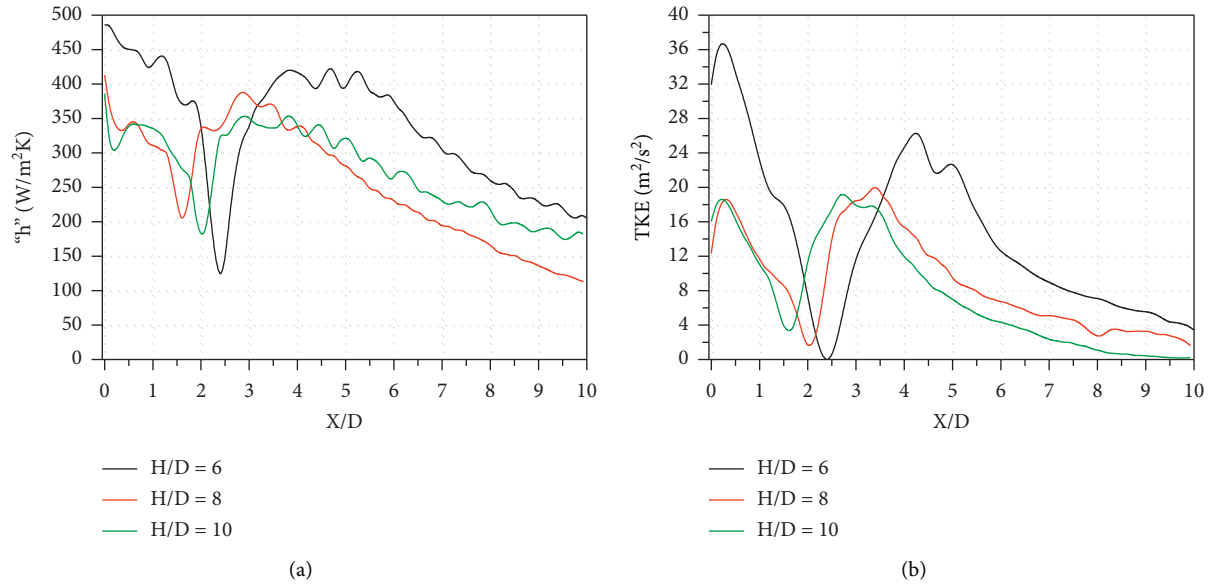

Figure 6: (a) Local heat transfer coefficient (W/m^2-K) and (b) turbulent kinetic energy (m^2/s^2) distribution at fixed "S/*D*" of 3 and "Re" of 11000 for varying separation distances, "H/*D*" of 6, 8, and 10.

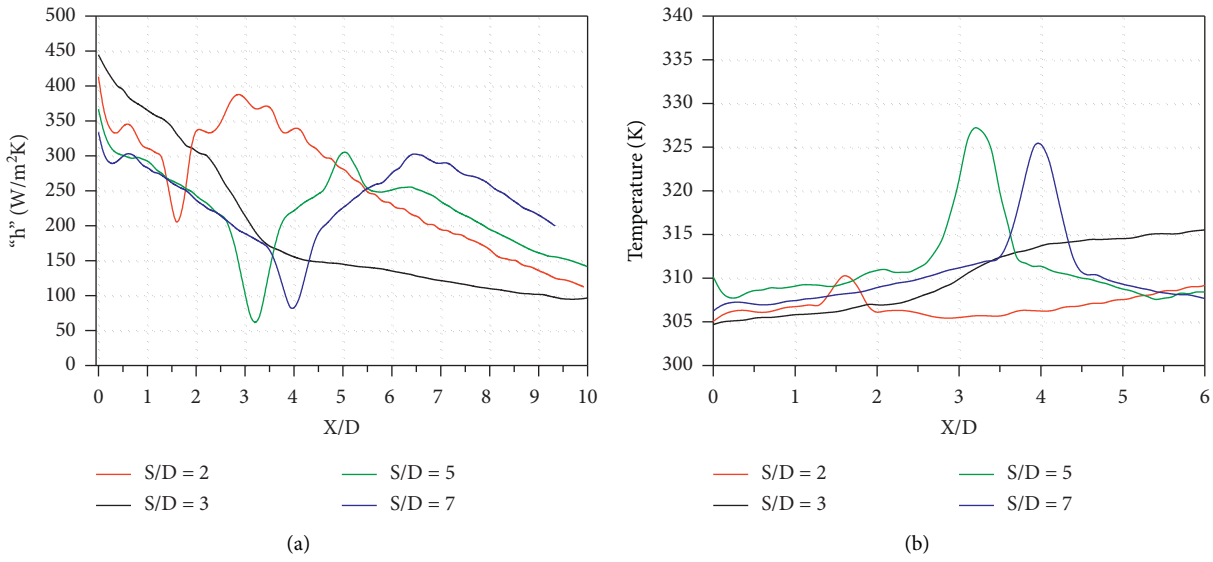

Figure 7: (a) Local heat transfer coefficient (W/m^2-K) and (b) temperature (K) distribution at fixed "H/*D*" of 8 and "Re" of 9000 for varying separation distances, "S/*D*" of 2, 3, 5, and 7.

varied as "Re" = 7000, 9000, and 11000. Experimental data analysis suggests a rise in the value of heat transfer rate and thus Nusselt number by increasing Reynolds number at same separation distance.

The impact of Reynolds number on coefficient of heat transfer and turbulent kinetic energy (TKE) is shown in Figure 8. For a fully developed pipe flow, Popiel and Boguslawski [35] revealed that the turbulent intensity as well as kinetic energy rises and achieves their maximum value at "H/*D*" = 6 for a single jet. This results from high turbulent jet intensity. Even though the jet centerline velocity starts decaying due to its interaction with the ambient, the turbulent intensity continues to increase. The outer peak in heat transfer distribution begins to become less distinctive because the rate of heat transfer at the impact region has developed to so high values that the chances of their further increase as an outcome of transition from laminar to turbulent flow are attenuated. The heat transfer coefficient value "h" at the stagnation region corresponding to central jet increases from 370 W/m^2-K to 495 W/m^2-K with the rise in Reynolds number. Rise in "Re" leads to increased length of potential core region, and thus the axial velocity at the jet centerline is preserved for much greater downstream distances. This marks the increase of heat transfer at the corresponding locations on the target plate. Variation of turbulent kinetic energy shows maximum turbulence at

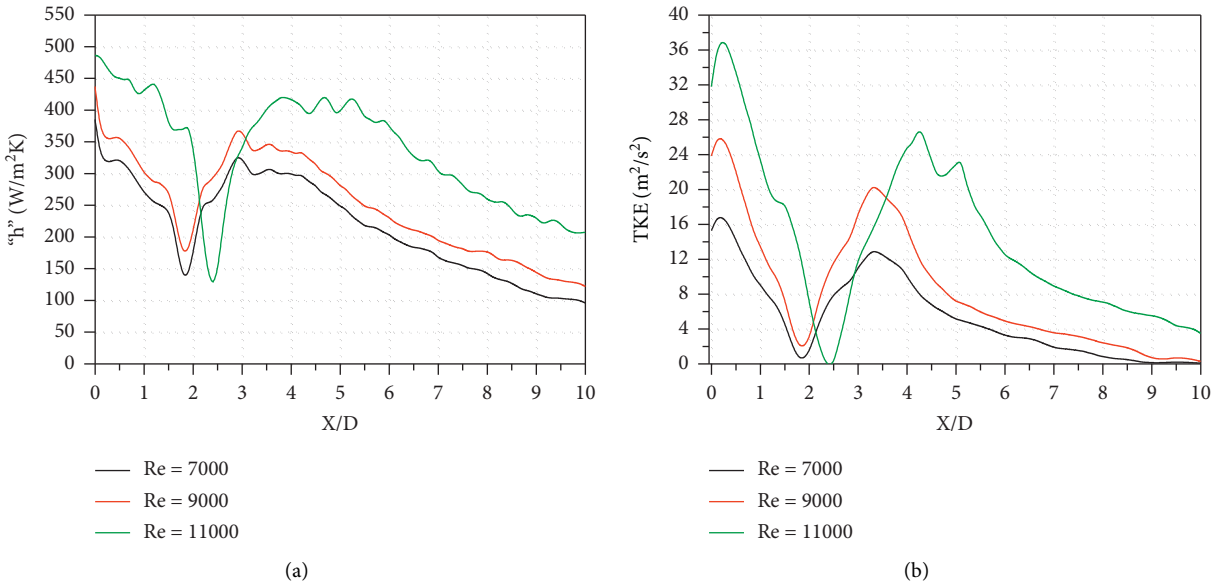

Figure 8: (a) Local heat transfer coefficient (W/m^2-K) and (b) turbulent kinetic energy (m^2/s^2) distribution at fixed "H/D" of 6 and "S/D" of 3 for varying "Re" of 7000, 9000, and 11000.

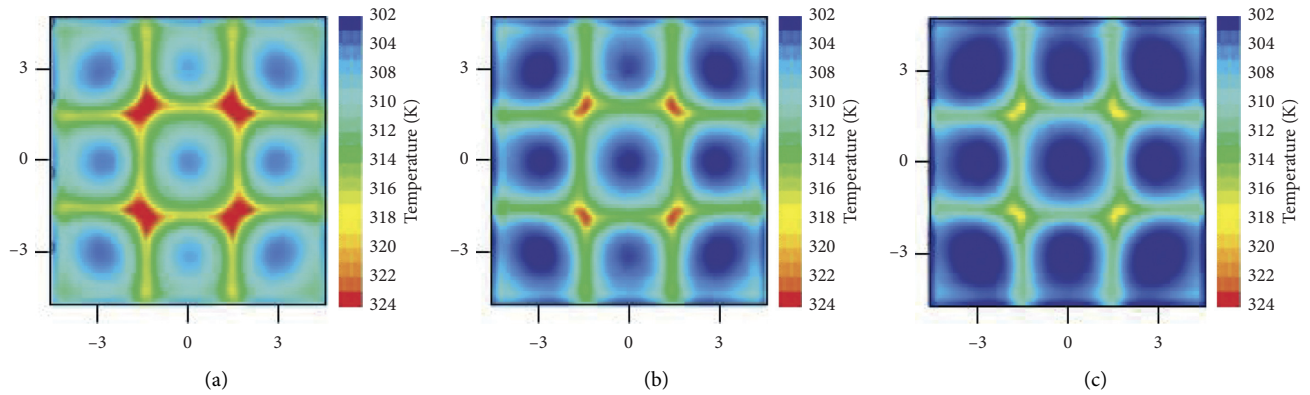

Figure 9: Local contours of temperature (K) developed at the target surface at separation distance "H/D" of 6 and inter-jet spacing "S/D" of 3 for different Reynolds number corresponding to (a) 7000, (b) 9000, and (c) 11000.

Table 4: Averaged heat transfer coefficients for various cases.

Cases	Re = 7000	Re = 9000	Re = 11000
H/D = 6	178 (W/m^2-K)	210 (W/m^2-K)	241 (W/m^2-K)
H/D = 8	174 (W/m^2-K)	204 (W/m^2-K)	219 (W/m^2-K)
H/D = 10	170 (W/m^2-K)	193 (W/m^2-K)	213 (W/m^2-K)
		Inter-jet spacing (S/D)	
Re = 9000 and H/D = 8	2	3	5	7
	205	204	200	182

regions confirming to the location of the jets. Turbulent kinetic energy has been found to be high at the stagnation regions corresponding to the jets, and the values of "TKE" increase from 15.2 m^2/s^2 to 31.8 m^2/s^2 at "X/D" = 0 with the rise in Reynolds number, "Re" from 7000 to 11000.

Figure 9 highlights the temperatures attained by the target plate at different values of Reynolds number for fixed "S/D" of 3 and "H/D" of 6. It can be seen that the plate becomes cooler particularly at the places related to stagnation regions of different impinging jets.

The plate, however, remains relatively hotter at the intersection regions developed in-between four jets and interaction areas in-between each pair of jets. The temperature values decrease from 324 K to 315 K at the regions corresponding to intersection of four jets with increasing values of Reynolds number.

3.4. Averaged Heat Transfer Coefficients "H_{avg}". Averaged heat transfer coefficients at the target surface are given in Table 4.

4. Concluding Remarks

Numerical modeling can be used as an alternative and powerful tool to predict the trend in variation of heat transfer rates as well as fluid flow features in various fluid flow applications. The trends obtained in the current numerical study show the effects of separation distance, inter-jet spacing, and Reynolds number on coefficient of heat transfer and turbulent kinetic energy. Following are the major concluding remarks:

(1) The "k-ω" SST model is observed to match best with the experimental data among different models selected for the study.

(2) The local "h" values have been noticed to decline with the rise in separation distance "H/D." The average value of heat transfer coefficient "h" reduces from 210 to 193 W/m^2-K with increase in "H/D" from 6 to 10 at "Re" = 9000 and S/D of 3.

(3) The values of coefficient of heat transfer "h" and thus Nusselt number rise due to the rise in Reynolds number "Re."

(4) The average value of coefficient of heat transfer "h" is 205, 204, 200, and 182 W/m^2-K at inter-jet spacing "S/D" of 2, 3, 5, and 7, respectively, at "H/D" = 8 and "Re" = 9000. At "S/D" = 2, the multiple jets start behaving as a large single jet.

(5) On the basis of heat transfer features, inter-jet spacing "S/D" = 3 has been determined to be the optimum value for increasing heat transfer.

Nomenclature

X, Y: Coordinate axis on impingement plate
X/D: Nondimensional x-distance
Y/D: Nondimensional y-distance
D: Diameter of nozzle (mm)
H: Impingement separation (mm)
H/D_h: Nondimensional impingement separation
S/D_h: Inter-jet spacing (dimensionless)
T: Temperature (K)
T_s: Surface temperature (K)
T_∞: Ambient temperature (K)
p: Pressure (Pa)
q''L: Heat flux (kW/m^2)
h_{avg}: Averaged heat transfer coefficient (W/m^2-K)
h: Convective heat transfer coefficient
Re: Reynolds number
u, v, w: Velocity components in x, y, and z directions (m/s)
k: Turbulent kinetic energy, TKE (m^2/s^2)
S_k: Source term for TKE
S_ω: Source term for "ω"
Y_k: Dissipation term for k in k-ω model
Y_ω: Dissipation term for ω in k-ω model
k_{eff}: Effective thermal conductivity (W/m-K)

Abbreviations

Nu: Nusselt number
RANS: Reynolds averaged NS equations
Re: Reynolds number
RNG: Renormalization group theory
STD: Standard
SST: Shear stress transport
TKE: Turbulent kinetic energy (W/m^2-K)

Greek Symbols

μ: Dynamic viscosity (kg/m-s)
ε: Dissipation rate (m^2/s^3)
ρ: Density (kg/m^3)
ω: Specific dissipation rate (m^2/s^4).

Data Availability

The data used to support the findings of this study are included within the article.

Conflicts of Interest

The authors declare that they have no conflicts of interest.

References

[1] M. Mirzaee, R. Zare, M. Sadeghzadeh, and H. Maddah, "Thermodynamic analyses of different scenarios in a CCHP system with micro turbine–absorption chiller, and heat exchanger," *Energy Conversion and Management*, vol. 198, 2019.

[2] M. Mehrpooya, M. Sadeghzadeh, A. Rahimi, and M. Pouriman, "Technical performance analysis of a combined cooling heating and power (CCHP) system based on solid oxide fuel cell (SOFC) technology-a building application," *Energy Conversion and Management*, vol. 198, Article ID 111767, 2019.

[3] S. Esbati, M. A. Amooie, M. Sadeghzadeh, M. H. Ahmadi, F. Pourfayaz, and T. Ming, "Investigating the effect of using PCM in building materials for energy saving: case study of Sharif Energy Research Institute," *Energy Science & Engineering*, vol. 1–14, 2019.

[4] R. Viskanta, "Heat transfer to impinging isothermal gas and flame jets," *Experimental Thermal and Fluid Science*, vol. 6, no. 2, pp. 111–134, 1993.

[5] N. Zuckerman and N. Lior, "Jet impingement heat transfer: physics, correlations, and numerical modeling," Edited by G. A. Greene, J. P. Hartnett, A. Bar-Cohen, and Y. I. B. T.-A. Cho, Eds., vol. 39, pp. 565–631, Elsevier, Amsterdam, Netherlands, 2006.

[6] D. E. Metzger and R. J. Korstad, "Effects of crossflow on impingement heat transfer," *Journal of Engineering for Power*, vol. 94, no. 1, pp. 35–41, 1972.

[7] C.-Y. Li and S. V. Garimella, "Prandtl-number effects and generalized correlations for confined and submerged jet

impingement," *International Journal of Heat and Mass Transfer*, vol. 44, no. 18, pp. 3471–3480, 2001.

[8] R. J. Goldstein and J. F. Timmers, "Visualization of heat transfer from arrays of impinging jets," *International Journal of Heat and Mass Transfer*, vol. 25, no. 12, pp. 1857–1868, 1982.

[9] A. I. Behbahani and R. J. Goldstein, "Local heat transfer to staggered arrays of impinging circular air jets," *Heat Transfer; Electric Power*, vol. 4, 1982.

[10] L. W. Florschuetz and C. C. Su, "Effects of crossflow temperature on heat transfer within an array of impinging jets," *Journal of Heat Transfer*, vol. 109, no. 1, pp. 74–82, 1987.

[11] N. T. Obot and T. A. Trabold, "Impingement heat transfer within arrays of circular jets: Part 1-effects of minimum, intermediate, and complete crossflow for small and large spacings," *Journal of Heat Transfer*, vol. 109, no. 4, pp. 872–879, 1987.

[12] R. J. Goldstein and W. S. Seol, "Heat transfer to a row of impinging circular air jets including the effect of entrainment," *International Journal of Heat and Mass Transfer*, vol. 34, no. 8, pp. 2133–2147, 1991.

[13] S. J. Slayzak, R. Viskanta, and F. P. Incropera, "Effects of interaction between adjacent free surface planar jets on local heat transfer from the impingement surface," *International Journal of Heat and Mass Transfer*, vol. 37, no. 2, pp. 269–282, 1994.

[14] A. M. Huber and R. Viskanta, "Effect of jet-jet spacing on convective heat transfer to confined, impinging arrays of axisymmetric air jets," *International Journal of Heat and Mass Transfer*, vol. 37, no. 18, pp. 2859–2869, 1994.

[15] J.-Y. San and M.-D. Lai, "Optimum jet-to-jet spacing of heat transfer for staggered arrays of impinging air jets," *International Journal of Heat and Mass Transfer*, vol. 44, no. 21, pp. 3997–4007, 2001.

[16] L. F. G. Geers, M. J. Tummers, and K. Hanjalic, "Experimental investigation of impinging jet arrays," *Experiments in Fluids*, vol. 36, no. 6, pp. 946–958, 2004.

[17] L. F. G. Geers, K. Hanjalić, and M. J. Tummers, "Wall imprint of turbulent structures and heat transfer in multiple impinging jet arrays," *Journal of Fluid Mechanics*, vol. 546, pp. 255–284, 2006.

[18] S. Spring, Y. Xing, and B. Weigand, "An experimental and numerical study of heat transfer from arrays of impinging jets with surface ribs," *Journal of Heat Transfer*, vol. 134, 2012.

[19] J.-Y. San and J.-J. Chen, "Effects of jet-to-jet spacing and jet height on heat transfer characteristics of an impinging jet array," *International Journal of Heat and Mass Transfer*, vol. 71, pp. 8–17, 2014.

[20] L. W. Florschuetz, C. R. Truman, and D. E. Metzger, "Streamwise flow and heat transfer distributions for jet array impingement with crossflow," *Journal of Heat Transfer*, vol. 103, no. 2, pp. 337–342, 1981.

[21] R. Gardon and J. C. Akfirat, "Heat transfer characteristics of impinging two-dimensional air jets," *Journal of Heat Transfer*, vol. 88, no. 1, pp. 101–107, 1966.

[22] J. Lee and S.-J. Lee, "The effect of nozzle configuration on stagnation region heat transfer enhancement of axisymmetric jet impingement," *International Journal of Heat and Mass Transfer*, vol. 43, no. 18, pp. 3497–3509, 2000.

[23] B. Weigand and S. Spring, "Multiple jet impingement-a review," in *Proceedings of the Int. Symp. Heat Transf. Gas Turbine Syst.*, pp. 2–4, Antalya, Turkey, August 2009.

[24] N. Chougule, G. Parishwad, P. R. Gore, S. Pagnis, and S. Sapali, "CFD analysis of multi-jet air impingement on flat plate," in *Proceedings of the World Congr Eng 2011, WCE*, vol. 3, pp. 2431–2435, London, UK, July 2011.

[25] S. Yong, Z. Jing-zhou, and X. Gong-nan, "Convective heat transfer for multiple rows of impinging air jets with small jet-to-jet spacing in a semi-confined channel," *International Journal of Heat and Mass Transfer*, vol. 86, pp. 832–842, 2015.

[26] A. Mahammedi, H. Ameur, Y. Menni, and D. M. Medjahed, "Numerical study of turbulent flows and convective heat transfer of Al2O3-water nanofluids in A circular tube," *Journal of Advanced Research in Fluid Mechanics and Thermal Sciences*, vol. 77, no. 2, pp. 1–12, 2020.

[27] Y. Menni, M. Ghazvini, H. Ameur, M. H. Ahmadi, M. Sharifpur, and M. Sadeghzadeh, "Numerical calculations of the thermal-aerodynamic characteristics in a solar duct with multiple V-baffles," *Engineering Applications of Computational Fluid Mechanics*, vol. 14, no. 1, pp. 1173–1197, 2020.

[28] H. Ameur, D. Sahel, and Y. Menni, "Enhancement of the cooling of shear-thinning fluids in channel heat exchangers by using the V-baffling technique," *Thermal Science and Engineering Progress*, vol. 18, Article ID 100534, 2020.

[29] N. Sakhri, Y. Menni, A. J. Chamkha et al., "Study of heat and mass transfer through an earth to air heat exchanger equipped with fan in South West of Algeria," *International Journal of Heat and Technology*, vol. 37, no. 3, pp. 689–695, 2019.

[30] H. Ameur and Y. Menni, "Non-Newtonian fluid flows through backward-facing steps," *SN Applied Sciences*, vol. 1, no. 12, Article ID 1717, 2019.

[31] H. Ameur and Y. Menni, "Laminar cooling of shear thinning fluids in horizontal and baffled tubes: effect of perforation in baffles," *Thermal Science and Engineering Progress*, vol. 14, Article ID 100430, 2019.

[32] N. Sakhri, Y. Menni, H. Ameur et al., "Investigation of the natural ventilation of wind catchers with different geometries in arid region houses," *Journal of Mechanical Engineering and Sciences*, vol. 14, no. 3, pp. 7109–7124, 2020.

[33] N. Sakhri, Y. Menni, and H. Ameur, "Experimental investigation of the performance of earth-to-air heat exchangers in arid environments," *Journal of Arid Environments*, vol. 180, Article ID 104215, 2020.

[34] S. V. Patankar, *Numerical Heat Transfer and Fluid Flow*, Routledge, London, UK, 1980.

[35] C. O. Popiel and L. Boguslawski, "Effect of flow structure on the heat or mass transfer on a lat plate in impinging round jet," in *Proceeding of International Heat Transfer Conference 5*, pp. 663–685, University of Strathclyde, Kyongju, Korea, August 1988.